# Supplementary Information

# Long-duration 3D single-molecule tracking reveals spatiotemporally heterogeneous biomolecular dynamics in condensates

Junhui Huang[1], Ran Liu[1,2], Yuxin Lin[3], Ziwei Shi[1,4,5], Yilin Tian[1,6], Shangguo Hou[1,4*]

[1] *Institute of Systems and Physical Biology, Shenzhen Bay Laboratory, Shenzhen 518132, China.*

[2] *School of Life Science and Technology, Harbin Institute of Technology, Harbin 150001, China*

[3] *Lyda Hill Department of Bioinformatics, UT Southwestern Medical Center, Dallas, TX 75390, USA*

[4] *Shenzhen Medical Academy of Research and Translation (SMART), Shenzhen 518107, China*

[5] *Westlake University, Hangzhou 310030, China*

[6] *University of Nottingham Ningbo China, Ningbo 315000, China*

Correspondence: Shangguo Hou, Shangguo.hou@szbl.ac.cn

# Supplementary Methods

## Tracking data analysis

Raw tracking data were used to reconstruct three-dimensional trajectories of individual tau molecules within condensates. Each trajectory contained time-dependent x, y, and z coordinates, together with photon-counting and timing information. For diffusion analysis, MSD curves were fitted with an anomalous diffusion model, $MSD(\tau) = 6D_{\alpha}\tau^{\alpha} + C$, to obtain the apparent diffusion coefficient and anomalous diffusion exponent.

## Recursive Bayesian reconstruction of three-dimensional trajectories

The reconstruction was performed using a recursive Bayesian approach adapted from previously reported methods[1]. Photon-event data acquired by the RT-3D-SPT system were divided into consecutive 100 μs intervals. The lateral and axial displacements of the particle relative to the feedback-controlled scan center were estimated using separate recursive Bayesian filters. Particle motion between adjacent intervals was described using a diffusion-based transition prior, and photon counts were modeled using a Poisson distribution. The posterior mode was taken as the estimated relative position in each interval and combined with the calibrated feedback-stage coordinates to obtain the absolute three-dimensional trajectory.

## HMM-based motion-state classification

For motion-state classification, diffusion parameters were calculated using 100 μs precision trajectory data with 200 ms stepping window and then were analyzed with hidden Markov model (HMM) analysis. HMMs with different numbers of hidden states were fitted, and the optimal model was selected based on the minimum Bayesian information criterion (BIC). Decoded states were assigned according to their relative mobility, and the resulting state sequences were used to analyze temporal changes in tau molecular motion within condensates.

## Residence mapping and hotspot identification

Residence maps were reconstructed from the three-dimensional trajectories to visualize spatial regions preferentially occupied by tau molecules within condensates. For two-dimensional projections, trajectory positions were projected onto the XY, XZ, and YZ planes and binned into

0.03 μm pixels. The residence signal in each bin was calculated from the number of trajectory points falling within that bin.

Reconstructed trajectories were segmented using sliding time windows, and the occupancy density and three-dimensional net displacement were calculated for each window. The occupancy density of each window was compared with the local background density. Windows showing background-corrected density enrichment and a net displacement below 400 nm were defined as hotspot candidates. The displacement threshold was set based on the spatial scale of restricted trajectory segments to exclude density enrichment caused by rapid passage through the condensate. Temporally adjacent hotspot candidate windows were merged into individual hotspot events when their window-center time interval was no greater than 0.50 s. For each hotspot event, the start time, end time, duration, peak occupancy density, mean occupancy density, background-corrected density enrichment, and corresponding net displacement were recorded. Hotspot annotations were then mapped back to the trajectory coordinates, local diffusion parameters, and HMM-decoded state sequences to compare molecular mobility and motion-state distributions inside and outside hotspot regions.

**Local drift field analysis**

To visualize local directional bias in molecular motion, a coarse-grained drift field was computed from lagged displacements in the xy plane. For each trajectory point, the displacement vector over a lag time of 20 ms was calculated, and these displacement vectors were assigned to the spatial bin corresponding to the starting position of the step. Within each spatial bin, the displacement vectors were averaged to calculate a local mean drift velocity vector. These vectors were overlaid on the corresponding occupancy map to assess whether local occupancy hotspots were associated with preferential return or convergent motion.

**Diffusion mapping**

Diffusion coefficients generated from HMM analysis were mapped spatially by assigning each $D$ to the mean position sampled during the corresponding 10-ms fitting window. The diffusion map was constructed on a 30-nm spatial grid by averaging all $D$ values assigned to each pixel. Pixels containing fewer than two diffusion estimates were excluded from display.

**Interface-associated trajectory analysis**

Interface-associated trajectories were identified from reconstructed three-dimensional trajectories, bright-field images, and trajectory density maps. Trajectory segments mainly distributed near the condensate periphery and showing ring-like or shell-like spatial patterns were classified as interface-associated trajectories, whereas trajectories distributed within the condensate interior without obvious boundary enrichment were used for comparison. To characterize the spatial distribution of interface-associated trajectories, three-dimensional trajectories were projected onto the XY, XZ, and YZ planes. Trajectory segments showing boundary-associated or shell-like distributions were fitted with circular or spherical shell models to estimate their radial distribution relative to the condensate center. Local diffusion parameters and trajectory density distributions were then mapped onto the same trajectories to compare interface-associated motion with motion in the condensate interior.

**Inter-condensate trajectory analysis**

Inter-condensate migration trajectories were identified by comparing reconstructed three-dimensional trajectories with the positions of condensates in bright-field images. Trajectories that passed sequentially through two neighboring condensate regions were first selected as candidate migration events. Candidate events were retained only when the trajectory was temporally continuous and showed a gradual spatial transition from one condensate region to another, reducing potential misclassification caused by transient trajectory jumps or localization noise. The temporal order and spatial path of the molecule leaving the initial condensate, passing through the transition region, and entering the target condensate were recorded. Three-dimensional displacement and local diffusion parameters were extracted for each region to compare molecular motion across different spatial stages.

**Identification of condensate-associated and inter-condensate states**

Three-dimensional tau trajectories acquired by 3D-SMART were analyzed at a temporal sampling interval of 1 ms. To identify spatially distinct condensate-associated states, localization coordinates were clustered using DBSCAN ($\varepsilon$ = 0.08 μm, which is selected based on localization precision, and minimum points = 8)[2]. The minimum number of points was determined from the characteristic Brownian diffusion time required for a freely diffusing particle to traverse the DBSCAN neighborhood radius, $\tau_\varepsilon \backsim \varepsilon^2/2nD$, where $D$ is the diffusion coefficient and $n$ is the number of spatial dimensions. For the example trajectory in Figure 5, the measured diffusion coefficient $D$ =

0.198 μm$^2$/sec, $n$ = 3, and $\varepsilon$ = 0.08 μm, this corresponds to approximately 5.4 localizations at 1-ms sampling interval. We therefore used a slightly more stringent threshold of 8 to identify regions of sustained local confinement.

The two dominant spatial clusters were assigned as condensate-associated states 1 and 2, whereas localizations not assigned to either cluster were initially labeled as state 0. Consecutive state-0 localizations bracketed by the same condensate state (e.g., 1–0–1 or 2–0–2) were treated as segmentation gaps within a single condensate-associated dwell event. In contrast, state-0 localizations bracketed by different condensate states (1–0–2 or 2–0–1) were classified as inter-condensate transition events. For dwell-time analysis, same-state segments separated by such segmentation gaps were grouped as a single dwell event, while the intervening state-0 frames themselves were excluded from the dwell duration. The duration of each inter-condensate passage was calculated from the number of consecutive transition-state frames multiplied by the 1-ms sampling interval.

**Estimation of tau-accessible condensate volume**

For each condensate-associated state, the three-dimensional localization coordinates assigned to that state were used to reconstruct the spatial volume explored by the tracked tau molecule. A three-dimensional alpha shape was generated from the localization point cloud, and the alpha radius was set to the smallest value that produced a single connected region. The volume enclosed by the resulting alpha shape was defined as the tau-accessible volume, $V_i$, of the corresponding condensate-associated state. This quantity represents the three-dimensional configurational space sampled by the tracked molecule rather than the total geometric volume of the condensate.

The robustness of the tau-accessible volume estimates to localization sampling was evaluated using equal-number subsampling and rarefaction analyses on the representative trajectory shown in **Figure 5** (**Supplementary Figure 10 c-d**). For equal-number subsampling, the condensate-associated state containing more localizations was randomly downsampled to match the number of localizations in the smaller state, and the accessible volumes were recalculated from the resulting 3D point clouds. This procedure was repeated 500 times. For rarefaction analysis, equal numbers of localizations were randomly sampled from both states over a range of sample sizes, and the accessible volumes and their ratio were recalculated for each subsample.

## Supplementary Figures

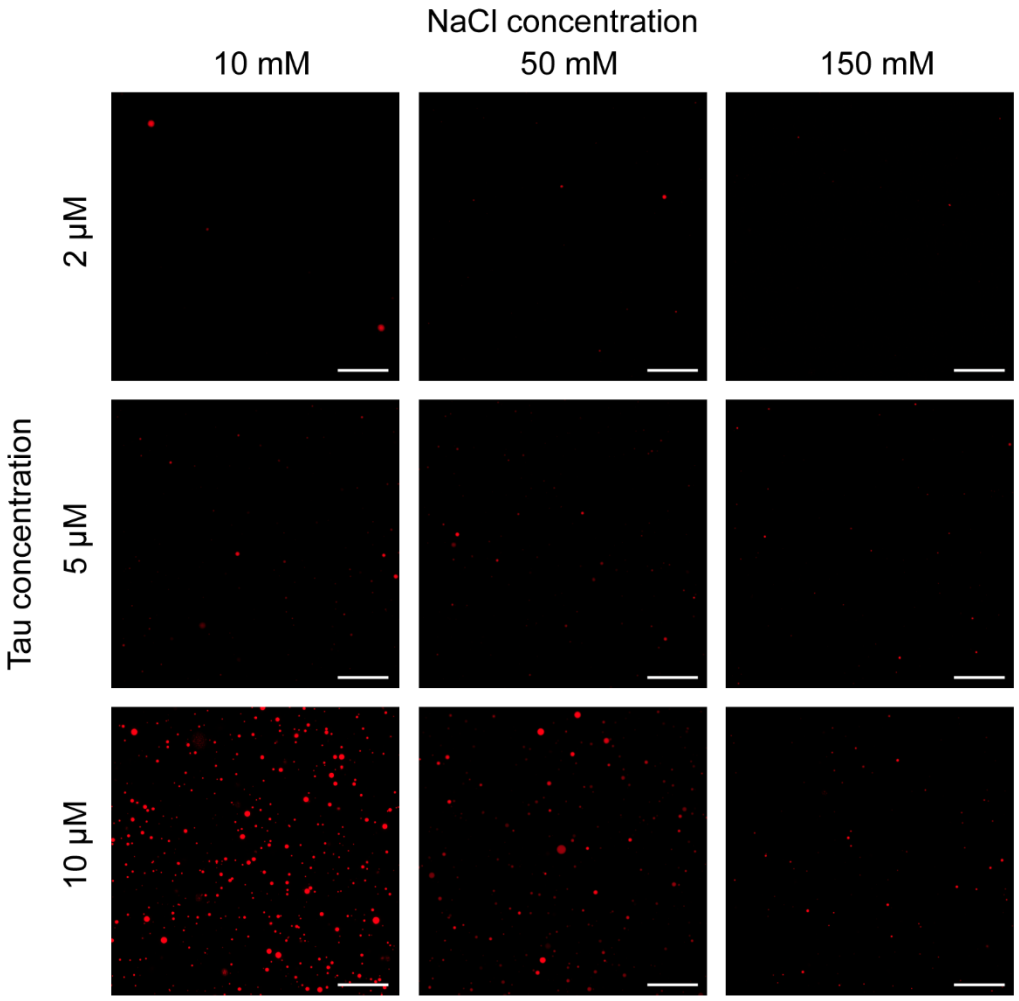


**Supplementary figure 1**. Confocal images of condensates at different tau concentrations of 2, 5 and 10 µM and NaCl concentrations of 10, 50 and 150 mM. Scale bars:10 µm.

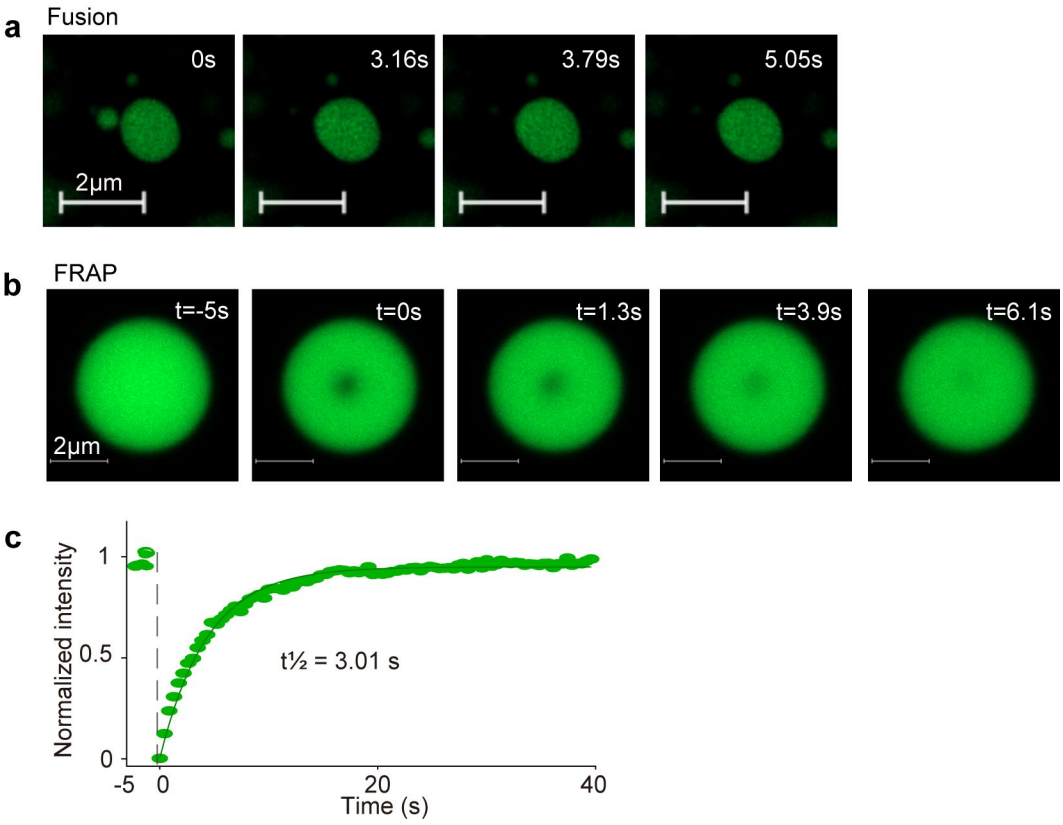


**Supplementary figure 2**. Characterization of tau condensates by fusion imaging and fluorescence recovery after photobleaching. (a) Time-lapse fluorescence images showing the fusion process of tau condensates. Scale bar: 2 μm. (b) Representative FRAP images of tau condensates. Scale bar: 2 μm. (c) Normalized fluorescence recovery curve derived from the FRAP image shown in (b). The recovery curve was fitted using an exponential model, yielding a half-recovery time (t1/2) of 3.01 s.

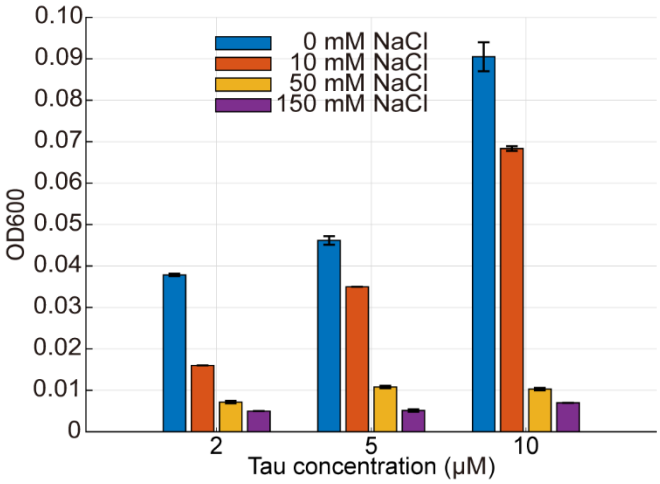


**Supplementary figure 3**. Turbidity of Tau condensates at different Tau concentration of 2, 5 and 10 µM and NaCl concentration of 0, 10, 50 and 150 mM.Sample were monitored by measuring the optical density at 600nm ($OD_{600}$). Measurements were collected every 3 min for 3 h. Bar shows the background-subtracted $OD_{600}$ values at the 3 h time point. Data are presented as the mean ± s.d. (n=2)

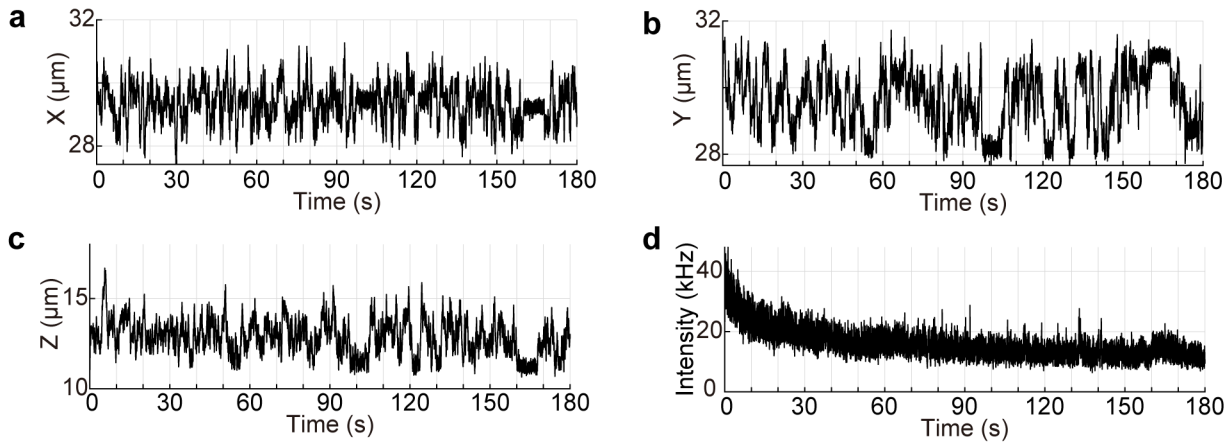


**Supplementary figure 4**. Spatial coordinates and intensity of the trajectory shown in main figure 2a. (a-c) x, y, z coordinates, respectively, as functions of time. (d) Intensity as a function of time.

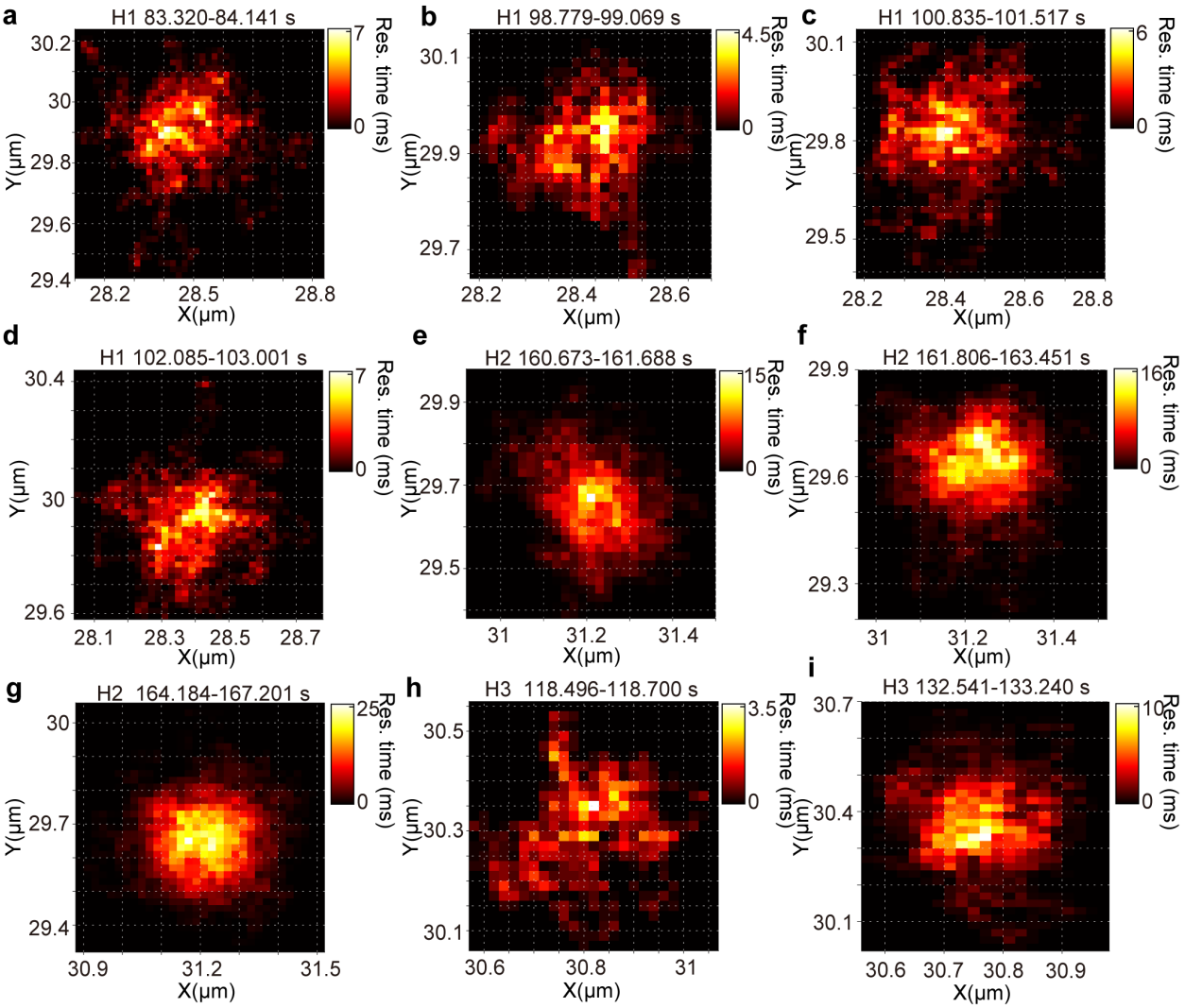


**Supplementary figure 5**. Representative hotspots visit events in areas H1–H3. The hotspots repeatedly appeared in the same area. (a–d) Hotspots repeatedly appeared in the H1 area in main figure 3a. The times shown above the figures indicate the corresponding time windows for these hotspots. There are more than ten hotspots visit events in the H1 area. Only four are shown here. (e–g) Hotspots repeatedly appeared in the H2 area in main figure 3a. (h, i) Hotspots repeatedly appeared in the H3 area in main figure 3a.

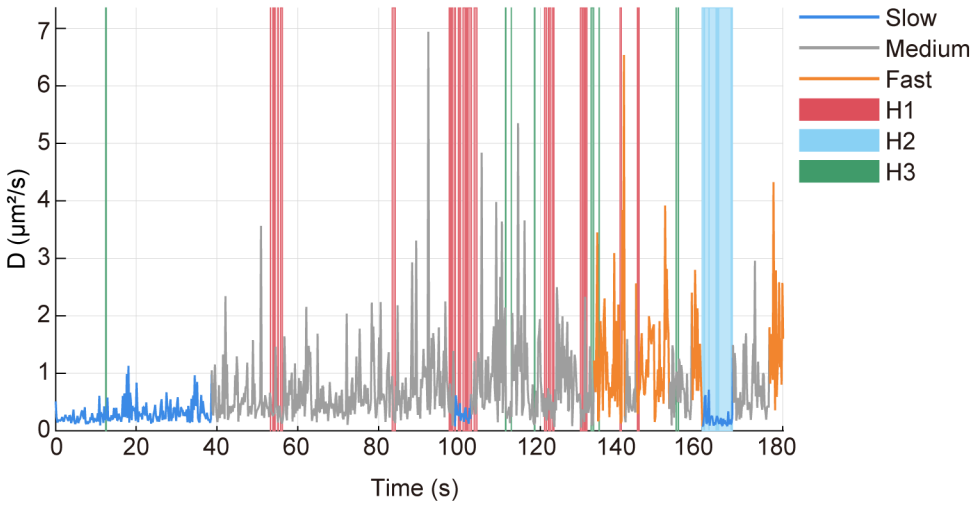


**Supplementary figure 6**. Time-dependent diffusion coefficient and hotspot visit events. The diffusion coefficient as a function of time for the trajectory shown in main figure 3a. The slow, medium, and fast states are plotted in blue, gray, and orange, respectively. The time windows of hotspot visit events are marked with red, light blue, and green for H1, H2 and H3, respectively.

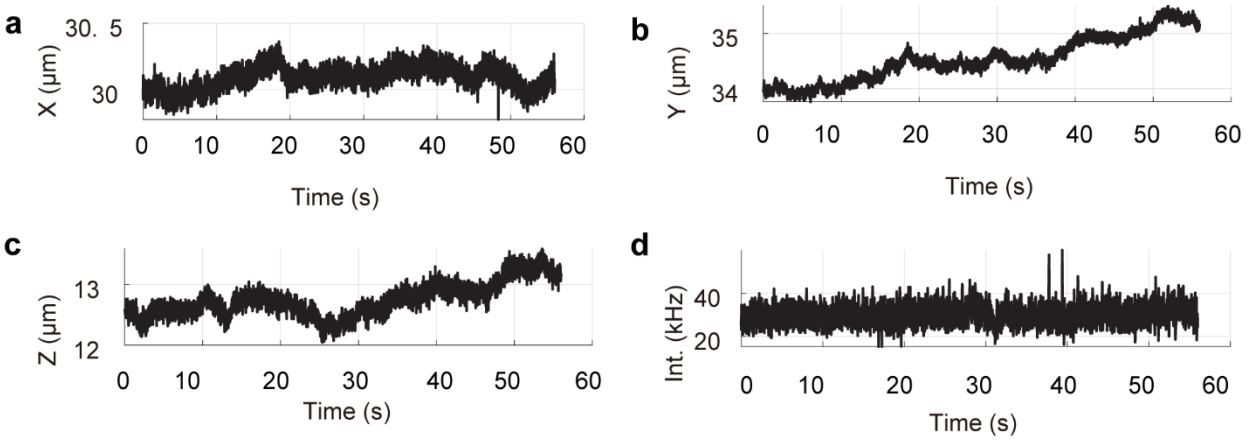


**Supplementary figure 7**. Spatial coordinates and intensity of the trajectory shown in main figure 4a. (a–c) x, y, z coordinates, respectively, as functions of time. (d) Intensity as a function of time.

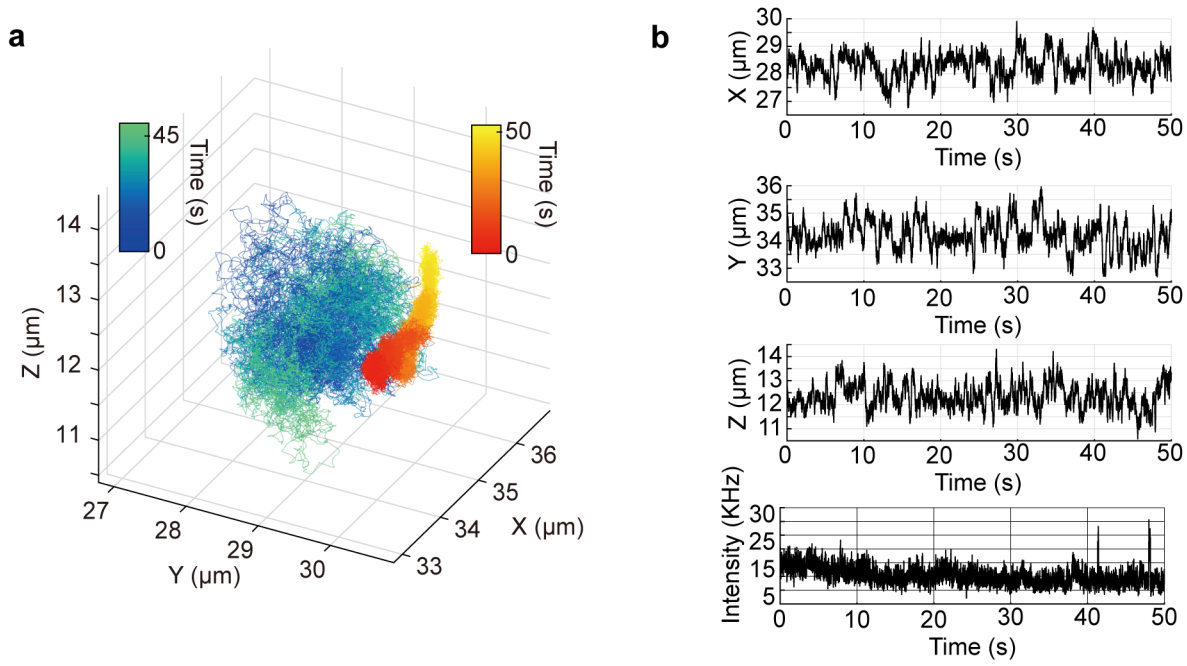


**Supplementary figure 8**. Comparison of two Tau trajectories within the same condensate. (a) The trajectory of tau near the boundary of condensate (red-to-yellow line) and the trajectory of tau inside of condensate (blue-to-green line). Both trajectories are color-coded by time. (b) The x, y, z, and intensity traces for the trajectory of tau inside of condensate.

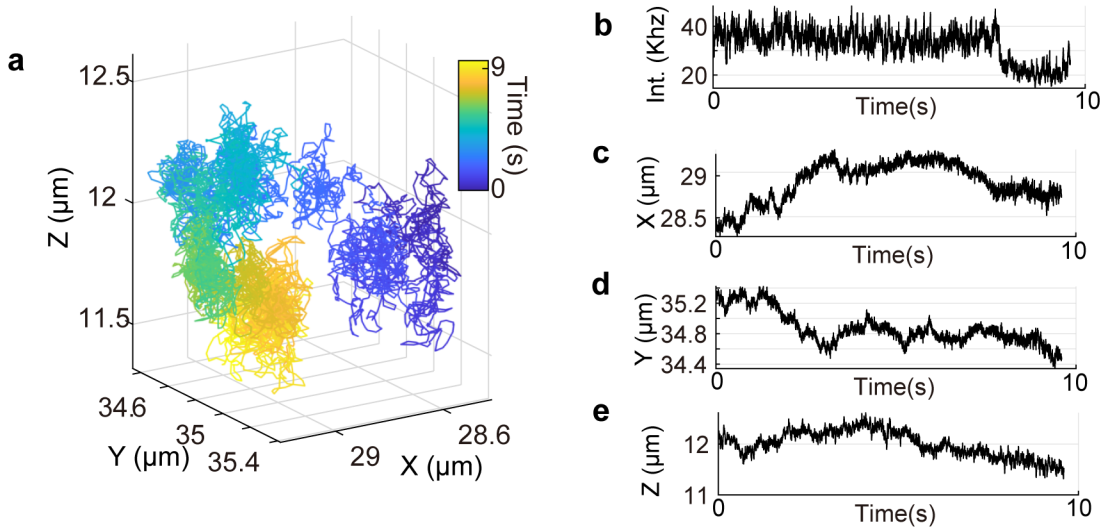


**Supplementary figure 9**. Additional boundary-associated tau trajectory. (a) Three-dimensional tau trajectory near the condensate boundary, color-coded by time. (b) Intensity as a function of time. (c–e) x, y, and z coordinates, respectively, as functions of time.

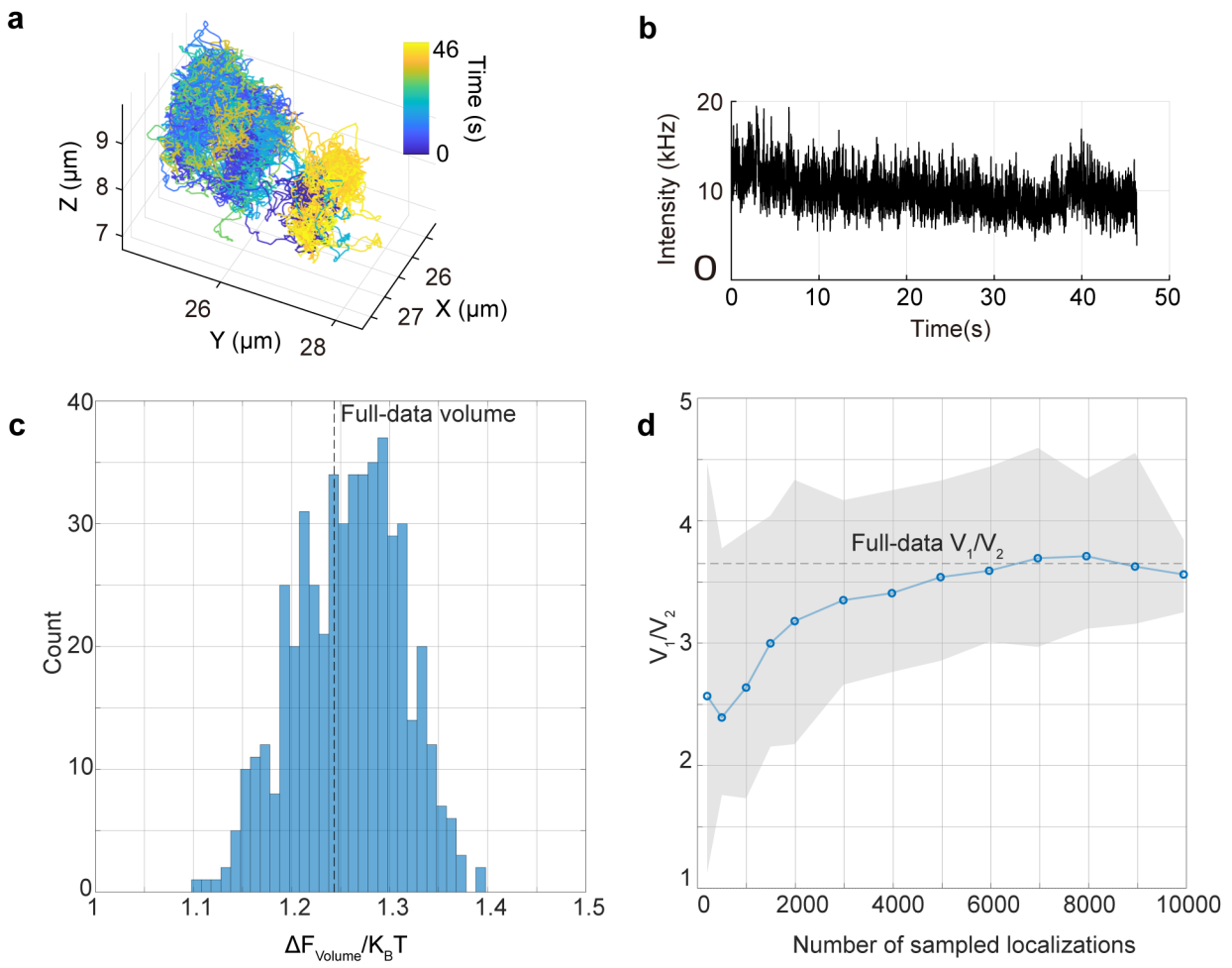


**Supplementary figure 10**. Three-dimensional trajectory with time coded by color (a) and the intensity trace (b) for the trajectory shown in figure 5. (c) Equal-number subsampling analysis of the volume-derived free-energy difference between the two condensate-associated states. The state containing more localizations was randomly downsampled to match the number of localizations in the smaller state, and tau-accessible volumes were recalculated from the resulting 3D point clouds using the alpha-shape procedure described in Methods. This procedure was repeated 500 times. The resulting volume-derived free-energy difference was 1.26 ± 0.05 $k_BT$ (mean ± s.d.), with a median of 1.26 $k_BT$ [2.5$^{th}$–97.5$^{th}$ percentile: 1.15–1.36 $k_BT$]. The dashed line indicates the value obtained from the full trajectory. (d) Convergence of the accessible-volume ratio with increasing localization numbers. Equal numbers of localizations were randomly sampled from the two condensate-associated states over a range of sample sizes, and the corresponding accessible volumes were independently reconstructed for each subsample. The shaded region indicates the 2.5$^{th}$–97.5$^{th}$ percentile empirical subsampling interval.

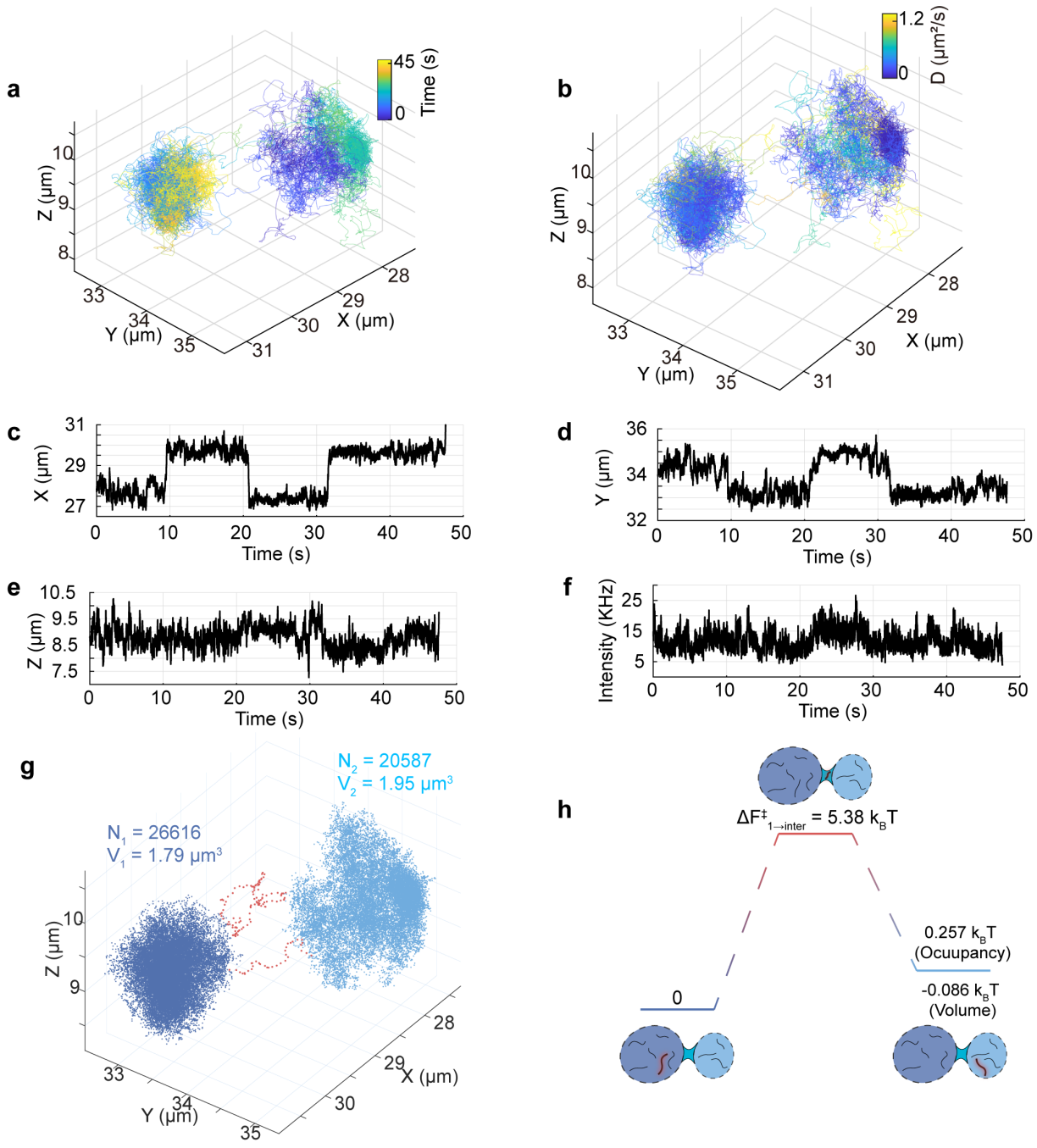


**Supplementary figure 11**. Additional trajectory shows the translocation of a single tau molecule between adjacent condensates. (**a**) Three-dimensional trajectory of condensate-to-condensate transfer event, color-coded by time. (**b**) Three-dimensional trajectory color-coded by apparent diffusion coefficient. (**c–f**) x, y, z, and intensity traces for trajectory shown in (**a**). (**g**) The point clouds of tau localizations from the trajectory shown in (**a**), assigned to condensate-associated states 1 and 2, and to the transition state, with corresponding numbers of localizations ($N$) and

accessible volumes ($V$). (**h**) Apparent free-energy diagram constructed from the relative occupancy of the trajectory-defined states, showing the free-energy difference between the two condensate-associated states and the apparent free-energy elevation associated with the inter-condensate transition state.

## References


1. Hou, S., Zhang, C., Niver, A. & Welsher, K.D. Mapping Nanoscale Forces and Potentials in Live Cells with Microsecond 3D Single-Particle Tracking. *Chemical & Biomedical Imaging* (2026).
2. Gan, J. & Tao, Y. in Proceedings of the 2015 ACM SIGMOD International Conference on Management of Data 519–530 (Association for Computing Machinery, Melbourne, Victoria, Australia; 2015).